*Journal of Applied Mechanics and Technical Physics, Vol. 51, No. 2, pp. 174–181, 2010*

# NUMERICAL STUDY OF A SWIRLED TURBULENT FLOW IN THE SEPARATION ZONE OF A CENTRIFUGAL AIR SEPARATOR

**A. V. Shvab, P. N. Zyatikov, Sh. R. Sadretdinov, and A. G. Chepel'**

UDC 532.517.4

*A mathematical model of a swirled turbulent flow in the separation zone of a pneumatic centrifugal device is presented. The model is based on the known $k$–$\omega$ model of turbulence proposed by Wilcox. The influence of rotation of the separation-zone walls, input swirl of the gas flow, and other characteristic parameters on the mean velocity field is demonstrated. A comparison of parameters is performed, which reveals good agreement between the numerical and experimental results for a turbulent fluid flow between parallel disks.*

**Key words:** *centrifugal air separator, swirled gas flow, separation zone, $k$–$\omega$ turbulence model, numerical simulation.*

**Introduction.** There are many various methods of separating disperse media. The most promising methods, however, seem to be centrifugal pneumatic methods, which can substantially increase the production efficiency, reduce energy expenses, and make the technological process of powder production more environmentally friendly.

Further improvement of the technological process of centrifugal separation of disperse media and creation of new effective devices for powder production are possible only on the basis of fundamental research in the field of hydrodynamics of one-phase and two-phase media in the field of centrifugal and aerodynamic forces with the use of mathematical models that describe these complicated phenomena.

There are two types of centrifugal devices designed for generating a swirled velocity field: devices that do not contain rotating elements [1] and devices that involve rotation of some parts of the separation chamber [2]. The use of rotating elements in the device makes it possible to obtain a more intense field of the circular component of velocity in the separation zone (which increases the efficiency of particle separation) and offers better control of this field. At the same time, the presence of rotating elements in the device involves an additional parameter, which complicates the study of swirled flow hydrodynamics, but simultaneously ensures additional possibilities of obtaining a more uniform field of centrifugal forces. Therefore, the present activities are mainly aimed at a detailed theoretical study of a swirled turbulent flow in the separation element of the centrifugal air separator, which is a specially designed test rig (Fig. 1) [3].

**1. Sketch of the Test Rig.** The test rig consists of a separation unit, which can be made in different variants, with axial and tangential injection of the initial material and air flow into the separation zone to ensure various variants of flow redistribution. The rig also includes a dispenser for the initial material, a dust-separation system (consisting of a cyclone collector and a filter), a control unit, an injection system (air duct or vacuum pump), and 12 swiveling nozzles, which serve to supply air with different degrees of swirling into the separation zone. To ensure pumping of air through the device, the test rig is connected to an air duct operating in the suction mode or to a VVN-3 water-ring vacuum pump. A two-channel control panel for single-type DC engines ensures regulation and stabilization of the rotation velocity of the spiral conveyor of the dispenser and the rotor of the centrifugal air separator in the range of 200 to 6000 rpm. The rotor velocity is additionally monitored by a stroboscope and recorded by a ChZ-33 frequency meter. The mass flow of air is measured by the method proposed in [4] and is

Tomsk State University, Tomsk 634050; shamil@sibmail.com; zpnpavel@sibmail.com. Translated from Prikladnaya Mekhanika i Tekhnicheskaya Fizika, Vol. 51, No. 2, pp. 39–48, March–April, 2010. Original article submitted February 19, 2009; revision submitted May 4, 2009.

 

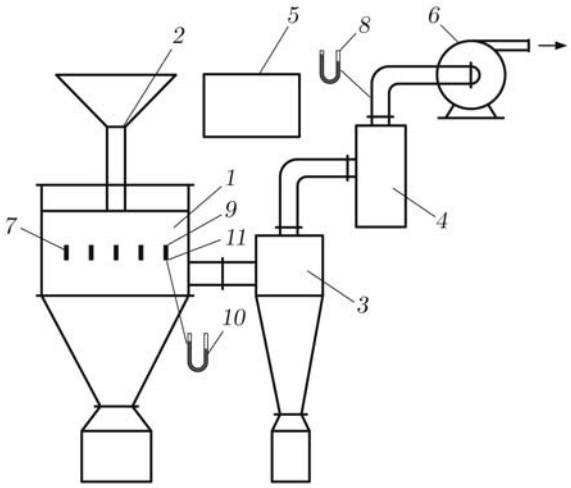


Fig. 1. Sketch of the test rig: separation unit (1), dispenser for the initial material (2), dust-separation system consisting of a cyclone collector (3) and a filter (4), control unit (5), injection device (6), swiveling nozzles (7), differential manometer (8), cylindrical probe (9), inclined differential manometer (10), and traversing gear (11).

registered by a differential manometer. A cylindrical probe connected to an inclined differential manometer and driven by a traversing gear is placed into the separation zone to determine the circular velocity component of the air flow. The cylindrical probe is made of a syringe needle with an outer diameter $d_1 = 1.2$ mm and an orifice diameter $d_2 = 0.5$ mm. Probe fabrication, its calibration, and measurements were performed in accordance with the method proposed in [4]. For this cylindrical probe, the calibration coefficient was 0.98. The probe was fixed on the device casing and could be moved by a special coordinate gear in the axial (the motion accuracy within $\pm 0.05$ mm) and angular (within 1°) directions of the separation zone.

The relative error of dynamic pressure measurements can be estimated by the formula

$$\frac{\Delta(\Delta P)}{\Delta P} = \frac{1}{\Delta P}\left(\Delta P_1 + \Delta P_2 + \left|\frac{dP}{dy}\right|\Delta y\right) \cdot 100\ \%,$$

where $\Delta P$ is the current pressure difference, $\Delta P_1$ is the absolute error due to the variations in the regime, $\Delta P_2$ is the absolute error due to inaccuracy of reading values on the measurement scale, and $|dP/dy|\,\Delta y$ is the absolute error due to inaccuracy of mounting of the pneumometric probe at a specified point. The measurement error of the airflow velocity components was smaller than 10%.

The separation unit of the centrifugal air separator is the main unit of the test rig and consists of the casing where a rotor including the upper contoured disk, a set of disks, and a shield are mounted on the shaft with a bearing unit. The upper contoured disk, the set of disks, the upper part of the rotor shield, and the upper edge of the guide funnel form the separation zone. The separator rotor set into motion with an electric drive is equipped with replaceable upper disks and additional inserts, which ensure variations of the separation element geometry in accordance with one of the three channel types: expanding toward the rotation center, plane–parallel, or constricting toward the rotation axis. The hydrodynamics of the separation element was studied for the following separator parameters: the angular velocity of rotation of the separation element was $\Omega_0 = 10$–$600$ sec$^{-1}$, the mass flow rate of the carrier medium $Q$ was varied in the range $5 \cdot 10^{-3}$–$5 \cdot 10^{-2}$ m$^3$/sec, the radius of the separation element $R_0 = 0.12$ m, and the air flow could be supplied axially or tangentially. The absolute values of the velocity vector $|V|$ were determined with the use of a cylindrical probe at the periphery, near the nozzles; depending on the gas flow rate $Q$, these values varied from 5 to 35 m/sec. For the amount of rotor rounds $N = 21$ sec$^{-1}$, the angle between the radius $R$ and the nozzle axis $\gamma = 60°$, and $Q = 1.39 \cdot 10^{-2}$, $3.50 \cdot 10^{-2}$, $4.20 \cdot 10^{-2}$, and $5.56 \cdot 10^{-2}$ m$^3$/sec, the following values were obtained: $|V| = 10.2$, 24.3, 28.9, and 37.0. Note that the angle $\gamma$ between the radius $R$ and the nozzle axis can take the values of 60°, 45°, and 0°.

The experimental data obtained are used to impose the boundary conditions in theoretical calculations of the carrier flow aerodynamics in the separation zone of the centrifugal air separator.

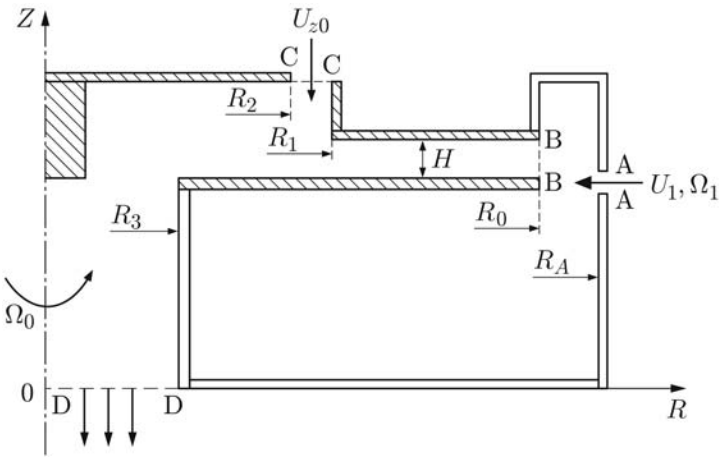


Fig. 2. Sketch of the separation element of the centrifugal air separator: the hatched areas are the rotating elements.

**2. Physical and Mathematical Formulation of the Problem.** The process of particle separation in terms of their size proceeds in the separation element schematically shown in Fig. 2. Through twelve $0.025 \times 0.005$ m rectangular-section nozzles located in the casing of the separation unit with a radius $R_A = 0.14$ m, the air flow with certain circular and radial velocity components enters the separation element with a radius $R_0 = 0.12$ m through the section B–B; the distance between the disks is $H = 0.01$ m. An additional air flow with the mean velocity $U_{z0} = \alpha U_0$ ($\alpha = 0.1$ is an experimental constant) is supplied into the separation element through the section C–C, which is a ring ($R_1 - R_2 = 0.005$ m). The powder is also supplied in this section, in addition to the carrier medium. Under the action of centrifugal and aerodynamic forces, the powder is separated into the coarse and fine fractions. The separation element rotates with an angular velocity $\Omega_0 = 10$–$600$ sec$^{-1}$.

During its motion in the separation element, the carrier flow acquires an additional momentum in the circular direction owing to rotation of the disk elements; after that, the carrier flow containing the fine fraction of the separated particles is brought away from the chamber through the section D–D in the axial area with a radius $R_3 = 0.035$ m. Obviously, with such organization of the carrier medium motion, the particles are separated into the fine and coarse fractions directly in the separation element. It seems reasonable to use the mean-mass-flow velocity $U_0 = Q/(2\pi R_0 H)$ and the distance between the disks $H$ as the basic velocity and length scales characterizing the swirled turbulent flow between the disk elements. Other parameters that exert a significant effect on the swirl flow dynamics are the angular velocity of separation element rotation $\Omega_0$ and the angular velocity of gas swirling induced by the nozzles; the mean angular velocity of swirling near the swiveling nozzles $\Omega_1 = U_\varphi/R_A$ ($U_\varphi$ is the mean circular component of velocity) is also estimated on the basis of experimental data.

The carrier medium is usually a gas or air moving with comparatively low velocities; therefore, a model of an incompressible fluid is used as a carrier medium model. It is convenient to perform this study in a cylindrical coordinate system $(r, \varphi, z)$. As the swirled gas flow rapidly acquires an axisymmetric character in the presence a large number of nozzles, we have the condition $\partial/\partial\varphi = 0$ owing to axial symmetry.

To describe the swirled turbulent motion, we use the system of the Reynolds equations written in a cylindrical coordinate system; this system is closed by the generalized Boussinesq hypothesis in which the Reynolds stresses are assumed to be proportional to the mean-flow strain rate.

To obtain dimensionless equations, we use the mean-mass-flow velocity $U_0$ as the velocity scale and the distance $H$ as the characteristic linear scale. Using these scales and also constant values of the gas density $\rho^0$ and kinematic viscosity $\nu^0$, we obtain the dimensionless values of pressure and turbulent viscosity $p = p^0/(\rho U_0^2)$ and $\nu_t = \nu_t^0/\nu^0$ ($p^0$ and $\nu_t^0$ are the dimensional values of pressure and turbulent viscosity).

With allowance for the axial symmetry and the generalized Boussinesq hypothesis, the Reynolds equations converted to the dimensionless and divergent forms are

$$\frac{\partial}{\partial r}(u_r r) + \frac{\partial}{\partial z}(u_z r) = 0; \tag{1}$$

$$\frac{\partial ru_r}{\partial\tau}+\frac{\partial}{\partial r}\left(ru_r^2\right)+\frac{\partial}{\partial z}\left(ru_zu_r\right)-\frac{1}{\mathrm{Re}}\Big[\frac{\partial}{\partial r}\Big(r(1+\nu_t)\,\frac{\partial u_r}{\partial r}\Big)+\frac{\partial}{\partial z}\Big(r(1+\nu_t)\,\frac{\partial u_r}{\partial z}\Big)\Big]$$

$$=u_\varphi^2-r\,\frac{\partial p}{\partial r}+\frac{r}{\mathrm{Re}}\Big(\frac{\partial\nu_t}{\partial r}\,\frac{\partial u_r}{\partial r}+\frac{\partial\nu_t}{\partial z}\,\frac{\partial u_z}{\partial r}-\frac{u_r}{r^2}\,(1+\nu_t)\Big),$$

$$\frac{\partial ru_z}{\partial\tau}+\frac{\partial}{\partial r}\left(ru_ru_z\right)+\frac{\partial}{\partial z}\left(ru_z^2\right)-\frac{1}{\mathrm{Re}}\Big[\frac{\partial}{\partial r}\Big(r(1+\nu_t)\,\frac{\partial u_z}{\partial r}\Big)+\frac{\partial}{\partial z}\Big(r(1+\nu_t)\,\frac{\partial u_z}{\partial z}\Big)\Big] \tag{2}$$

$$=-r\,\frac{\partial p}{\partial z}+\frac{r}{\mathrm{Re}}\Big(\frac{\partial\nu_t}{\partial r}\,\frac{\partial u_r}{\partial z}+\frac{\partial\nu_t}{\partial z}\,\frac{\partial u_z}{\partial z}\Big),$$

$$\frac{\partial ru_\varphi}{\partial\tau}+\frac{\partial}{\partial r}\left(ru_ru_\varphi\right)+\frac{\partial}{\partial z}\left(ru_zu_\varphi\right)-\frac{1}{\mathrm{Re}}\Big[\frac{\partial}{\partial r}\Big(r(1+\nu_t)\,\frac{\partial u_\varphi}{\partial r}\Big)+\frac{\partial}{\partial z}\Big(r(1+\nu_t)\,\frac{\partial u_\varphi}{\partial z}\Big)\Big]$$

$$=-u_ru_\varphi-\frac{1}{\mathrm{Re}}\Big((1+\nu_t)\,\frac{u_\varphi}{r}+u_\varphi\,\frac{\partial\nu_t}{\partial r}\Big).$$

Here, $u_r$, $u_z$, and $u_\varphi$ are the dimensionless components of the velocity vector, $r$ and $z$ are the dimensionless coordinates obtained with the use of the velocity scale $U_0$ and the length scale $H$, $\tau=tU_0/H$ is the dimensionless time, and $\mathrm{Re}=U_0H/\nu^0$.

To obtain a unique solution, system (1), (2) should be closed by appropriate boundary conditions. At the device entrance (section A–A) (see Fig. 2), the averaged values of the radial and circular velocity components are defined as constant values obtained on the basis of experimental data. The Neumann conditions, i.e., the zero value of the derivative $\partial/\partial z=0$, are imposed for all variables at the computational domain exit (section D–D). The no-slip condition is used on the solid walls of the separation zone, which implies that the radial and axial velocity components are equal to zero. For the circular velocity component, we have $u_\varphi=\mathrm{Rg}$ at the device entrance and $u_\varphi=\mathrm{Rn}\,R/R_0$ on the rotating surfaces [$\mathrm{Rg}=R_{\mathrm{A-A}}\Omega_1/U_0$ and $\mathrm{Rn}=R_0 2\pi N/(60U_0)=R_0\Omega_0/U_0$ are the dimensionless complexes (inverse Rossby criteria), $R_{\mathrm{A-A}}$ is the radius of the entrance section A–A (see Fig. 2), $R_0$ is the radius of the rotating disk, and $N$ is the number of round per minute of the separator disks]. Thus, we have three independent criteria: the Reynolds number Re and the rotation parameters Rg and Rn, which are actually the dimensionless values of the angular velocities of the rotor and gas entering the device from the nozzles.

**3. Turbulence Model.** There are several approaches to modeling turbulent viscosity. In this work, we use the differential $k$–$\omega$ turbulence model proposed by Wilcox [5], which includes two additional equations for transport of the kinetic energy of turbulent oscillations $k$ and the specific dissipation rate of the kinetic energy $\omega$. These equations have the following form in the cylindrical coordinate system with allowance for axial symmetry:

$$\frac{\partial rk}{\partial\tau}+\frac{\partial}{\partial r}\left(ru_rk\right)+\frac{\partial}{\partial z}\left(ru_zk\right)$$

$$=\frac{1}{\mathrm{Re}}\Big[\frac{\partial}{\partial r}\Big(r(1+\nu_t\sigma^*)\,\frac{\partial k}{\partial r}\Big)+\frac{\partial}{\partial z}\Big(r(1+\nu_t\sigma^*)\,\frac{\partial k}{\partial z}\Big)\Big]+G-\beta^*rk\omega,$$

$$\frac{\partial r\omega}{\partial\tau}+\frac{\partial}{\partial r}\left(ru_r\omega\right)+\frac{\partial}{\partial z}\left(ru_z\omega\right)$$

$$=\frac{1}{\mathrm{Re}}\Big[\frac{\partial}{\partial r}\Big(r(1+\nu_t\sigma)\,\frac{\partial\omega}{\partial r}\Big)+\frac{\partial}{\partial z}\Big(r(1+\nu_t\sigma)\,\frac{\partial\omega}{\partial z}\Big)\Big]+\gamma G\,\frac{\omega}{k}-\beta r\omega^2, \tag{3}$$

$$G=\frac{\nu_t r}{\mathrm{Re}}\Big\{\Big(\frac{\partial u_\varphi}{\partial r}-\frac{u_\varphi}{r}\Big)^2+\Big(\frac{\partial u_r}{\partial z}+\frac{\partial u_z}{\partial r}\Big)^2+\frac{\partial u_\varphi}{\partial z}+2\Big[\Big(\frac{\partial u_r}{\partial r}\Big)^2+\Big(\frac{u_r}{r}\Big)^2+\Big(\frac{\partial u_z}{\partial z}\Big)^2\Big]\Big\},$$

$$\nu_t=\mathrm{Re}\,k/\omega.$$

Here, $k=k^0/U_0^2$, $\omega=\omega^0H/U_0$, $k^0$, $\omega^0$ and $k$, $\omega$ are the dimensional and dimensionless kinetic energy and specific dissipation rate, respectively, and $\beta=3/40$, $\beta^*=9/100$, $\gamma=5/9$, $\sigma=1/2$, and $\sigma^*=1/2$ are constants [5].

The boundary conditions for the quantities $k$ and $\omega$ at the device entrance (section A–A) (see Fig. 2) are determined on the basis of experimental data for swirled flows. In particular, the kinetic energy of oscillatory motion was taken to be $k=0.1$ and the turbulent viscosity was $\nu_t=0.08\,\mathrm{Re}$. Based on these data, we determined the

specific dissipation rate $\omega = \mathrm{Re}\, k/\nu_t$ of the turbulence model (3). The Neumann conditions $\partial/\partial z = 0$ are imposed for $k$ and $\omega$ at the exit; the kinetic energy of turbulent oscillations on the solid boundaries is equal to zero by virtue of the no-slip condition. The specific dissipation rate $\omega$ on the solid surface can be obtained from the initial transport equation. In this case, the boundary condition for the specific dissipation rate on the solid wall reduces to the balance between molecular diffusion and dissipation. Depending on orientation of the radial or axial boundary, we obtain the corresponding conditions:

$$\frac{\partial}{\partial r}\Big(r\,\frac{\partial\omega}{\partial r}\Big) = r\,\mathrm{Re}\,\beta\omega^2, \qquad \frac{\partial^2\omega}{\partial z^2} = \mathrm{Re}\,\beta\omega^2. \tag{4}$$

As $r \to r_w$ and $z \to z_w$, the solution of Eqs. (4) has the form

$$\omega \xrightarrow{r\to r_w} \frac{4}{\mathrm{Re}\,\beta(r-r_w)^2}, \qquad \omega \xrightarrow{z\to z_w} \frac{6}{\mathrm{Re}\,\beta(z-z_w)^2},$$

where the subscript $w$ refers to the coordinates on the wall.

Thus, Eqs. (1)–(3) with appropriate boundary conditions form a closed system of differential equations that describe a swirled turbulent flow of an incompressible fluid.

**4. Method of the Solution.** The system of equations derived was solved numerically in the velocity–pressure physical variables by means of physical splitting of the velocity and pressure fields [6]. According to this method, solving the Reynolds equations written in the vector form includes two stages:

$$\frac{\boldsymbol{V}^+ - \boldsymbol{V}^n}{\Delta\tau} = -\nabla p^n + F(\boldsymbol{V}^+, \boldsymbol{V}^n); \tag{5}$$

$$\frac{\boldsymbol{V}^{n+1} - \boldsymbol{V}^+}{\Delta\tau} = -\nabla\,(\Delta p). \tag{6}$$

Equation (5) is actually system (2) written in the symbolic and vector form. The plus superscript indicates an intermediate grid function for the velocity vector; $\Delta p = p^{n+1} - p^n$ is a correction to pressure. Multiplying Eq. (6) by the gradient and taking into account the solenoid character of the velocity vector at the $(n+1)$th time layer, we obtain the Poisson equation for determining the correction to pressure:

$$\nabla^2(\Delta p) = \frac{\nabla\cdot\boldsymbol{V}^+}{\Delta\tau}. \tag{7}$$

The stationary problem is solved by a time-dependent method; therefore, dependence (7) is written in the form of a nonstationary differential equation

$$\frac{\partial\,\Delta p}{\partial\tau_0} - \nabla^2(\Delta p) = -\frac{\nabla\cdot\boldsymbol{V}^+}{\Delta\tau}, \tag{8}$$

where the fictitious time $\tau_0$ is an iteration parameter. In solving Eq. (8), we can write $\Delta\tau_0 = A\Delta\tau$ for the time step; the value of the constant $A$ is usually smaller than unity and is chosen from the condition of rapid convergence of the numerical process. The boundary condition for the correction to pressure is the Neumann condition, which is satisfied in the case if the exact value $\boldsymbol{V}^{n+1}$ is used for $\boldsymbol{V}^+$ at the boundary [7, 8].

Thus, system (5) is first solved by a time-dependent method, then Eq. (8) is solved, and finally the velocity vector at the $(n+1)$th time step and the pressure $p^{n+1} = p^n + \Delta p$ are found with the use of Eq. (6).

Using the method of splitting of the velocity and pressure fields, we obtain system (2), (3), (8), where each equation is the transport equation for a scalar quantity written in the conservative divergent form. The transport equation is solved on a hybrid staggered difference grid by the control volume method. The convective and diffusive terms of this equation are presented in finite differences with an exponential scheme [8], which ensures the second order of accuracy in terms of the coordinates and eliminates the constraint on the grid Reynolds number. In particular, for the sought variable $\Phi$, the convective and diffusive terms of the transport equation in the projection, for instance, onto the $r$ axis at the $(n+1)$th time layer are written in the following form with the use of the exponential scheme:

$$\frac{\partial}{\partial r}\,(ru_r\Phi) - \frac{\partial}{\partial r}\Big(\frac{r}{\mathrm{Re}}\,(1+\nu_t)\,\frac{\partial\Phi}{\partial r}\Big) = -A_i\Phi^{n+1}_{i-1,j} + B_i\Phi^{n+1}_{i,j} - C_i\Phi^{n+1}_{i+1,j}. \tag{9}$$

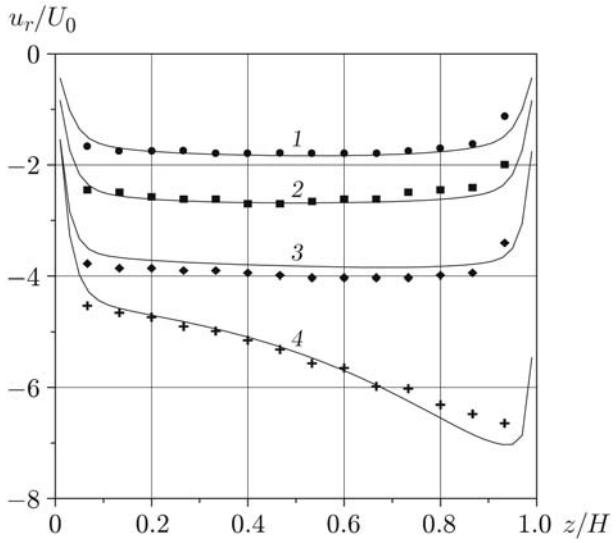


Fig. 3. Dimensionless radial velocity component versus the dimensionless coordinate $z/H$ for different values of the radius: the curves and points are the calculated results and the experimental data [11] for $r/r_0 = 0.600$ (1), 0.400 (2), 0.275 (3), and 0.185 (4).

Here, $i$ and $j$ are the subscripts of the difference grid points over the $r$ and $z$ coordinates; the coefficients $A$, $B$, and $C$ are found by the formulas

$$A_i = \frac{u_{r(-)}}{\Delta r}\,\frac{E_-}{E_- - 1}, \qquad C_i = \frac{u_{r(+)}}{\Delta r\,(E_+ - 1)}, \qquad B_i = A_i + C_i + \frac{u_{r(+)} - u_{r(-)}}{\Delta r},$$

$$E_+ = \exp\Big(\frac{\mathrm{Re}\,(ru_r)_+\Delta r}{[r(1+\nu_t)]_+}\Big), \qquad E_- = \exp\Big(\frac{\mathrm{Re}\,(ru_r)_-\Delta r}{[r(1+\nu_t)]_-}\Big);$$

the plus and minus indicate the values of the function at the control volume boundary on the right and left of this volume, respectively. For a uniform difference grid, for instance, this means that $u_{r(+)} = [(u_r)_{i,j} + (u_r)_{i+1,j}]/2$. It should be noted that there is a singularity of the form $0/0$ for the coefficient $C_i$ in the case with $u_{r(+)} = 0$. Expanding this singularity into an exponential series, we obtain

$$C_i = \frac{(1+\nu_t)_+}{\Delta r\,\mathrm{Re}}.$$

A similar result is obtained for the coefficient $A_i$.

The transport equation for the quantity $\Phi$ was solved numerically with the use of an implicit generalized scheme with variable directions. Let the transport equation have the form

$$\frac{\partial\Phi}{\partial\tau} = \Lambda_r\Phi + \Lambda_z\Phi + W, \tag{10}$$

where $\Lambda_r$ and $\Lambda_z$ are the operators of the convective-diffusive terms of the type (9) in the projections onto the $r$ and $z$ axes, respectively. To obtain a solution of the second-order accuracy in time, we write Eq. (10) in the $\Delta$-form at the time $n + 1/2$:

$$\frac{\Delta\Phi}{\Delta\tau} - \frac{1}{2}\,(\Lambda_r + \Lambda_z)\Delta\Phi = (\Lambda_r + \Lambda_z)\Phi^n + W.$$

Using approximate factorization [9], we obtain a two-stage algorithm:

$$\frac{\Delta\Phi^*}{\Delta\tau} - \frac{1}{2}\,\Lambda_r(\Delta\Phi^*) = (\Lambda_r + \Lambda_z)\Phi^n + W, \qquad \frac{\Delta\Phi^{**}}{\Delta\tau} - \frac{1}{2}\,\Lambda_z(\Delta\Phi^{**}) = \frac{\Delta\Phi^*}{\Delta\tau}, \qquad \Phi^{n+1} = \Phi^n + \Delta\Phi^{**}.$$

At each time step, we have a tridiagonal system of algebraic equations, which is solved by a sweep method.

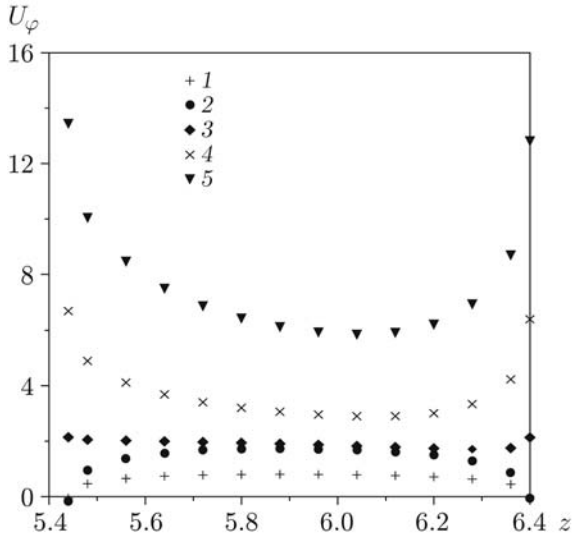


Fig. 4. Circular velocity component versus the $z$ coordinate in the section B–B at Re = 3733 and different values of the swirl parameters: 1) Rn = 0 and Rg = 4.05; 2) Rn = 0 and Rg = 5.43; 3) Rn = 2.14 and Rg = 4.05; 4) Rn = 6.42 and Rg = 4.05; 5) Rn = 12.85 and Rg = 4.05.

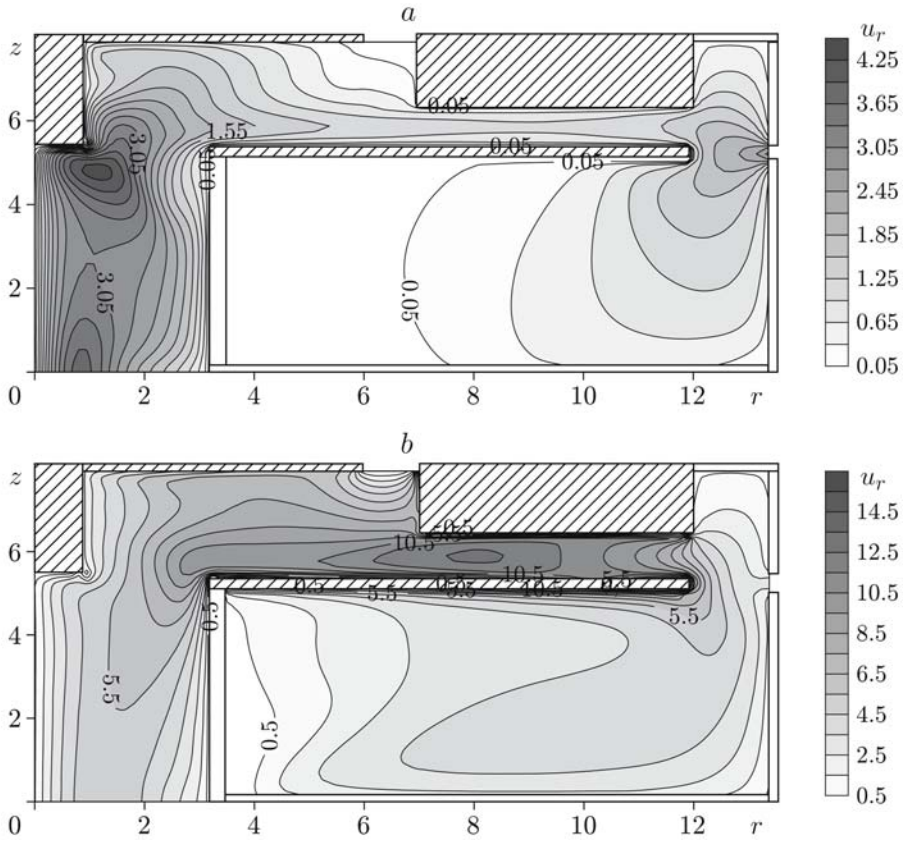


Fig. 5. Isolines of the circular velocity component at Re = 3733 and different flow parameters: (a) Rn = 0 and Rg = 4.05; (b) Rn = 12.85 and Rg = 4.05.

**5. Calculation Results.** The reliability and efficiency of the method developed was verified through test and numerical calculations [10] and also through comparisons with the experimental data [11] for a turbulent flow between plane–parallel disks in the direction from the periphery toward the axis. The experimental data [11] are compared in Fig. 3 with the calculated dependence of the dimensionless radial velocity component $u_r/U_0$ ($U_0$ is the constant value of the radial velocity at the entrance to the spatial area between the disks) on the dimensionless coordinate $z/H$ at $r_0/H = 10$, $\mathrm{Re} = U_0 H/\nu^0 = 1269$, and different values of the radius.

The analysis of available numerical solutions and experimental data for centrifugal air separators reduces mainly to studying the mean velocity fields in the area between the disks, because it is in this zone that the initial powder is separated into the fine and coarse fractions. These studies usually imply that the radial and circular velocity components change insignificantly at the entrance to this area between the disks (section B–B in Fig. 2). The present numerical study performed with the use of the mathematical model developed for a more general geometrical area including the peripheral region (from the section A–A to the section B–B) revealed significant nonuniformity of the distributions of the radial, circular, and axial velocity components in the section B–B and the effect of this nonuniformity on the subsequent dynamics of the swirled turbulent flow directly in the separation zone (Fig. 4). Figure 4 shows the profile of the circular velocity component in the entrance section B–B (see Fig. 2) with a constant flow rate of the fluid, $\mathrm{Re} = 3733$, and different values of the swirl parameters Rg and Rn.

Figure 5 shows the fields of the circular velocity component in the examined domain. The isolines of the circular velocity component are shown for the case without rotor rotation ($\mathrm{Rn} = 0$) in Fig. 5a and with a significant angular velocity of rotation of the disk elements ($\mathrm{Rn} = 12.85$, which corresponds approximately to 6000 rpm) in Fig. 5b. It follows from the analysis of Fig. 5 that the circular velocity component can substantially increase in the area between the disks, where the powder is separated into the fine and coarse fractions. Obviously, it becomes possible, on the one hand, to control the decrease in the marginal size of particles and, on the other hand, to obtain more uniform fields of the velocity vector in the separation zone of the centrifugal air separator.

**Conclusions.** A mathematical model is developed for calculating the hydrodynamics of a swirled turbulent flow formed in a centrifugal air separator. The main features of this flow are detected. The peripheral region is demonstrated to exert a significant effect on the aerodynamics in the separation zone of the centrifugal device. The mathematical model developed makes it possible not only to study the complicated pattern of the swirled turbulent flow, which is helpful for the development of new promising methods of powder separation, but also to optimize the operation and geometric parameters of the existing facilities.

## REFERENCES


1. V. E. Mizonov and S. G. Ushakov, *Aerodynamic Separation of Powders* [in Russian], Khimiya, Moscow (1989).
2. A. T. Roslyak, Yu. A. Biryukov, and V. N. Pachin, *Pneumatic Methods and Facilities for the Powder Technology* [in Russian], Izd. Tomsk. Univ., Tomsk (1990).
3. A. T. Roslyak, P. N. Zyatikov, V. K. Nikul'chikov, and Yu. A. Biryukov, "Method of separation of fine-grain materials and corresponding device," USSR Inventor's Certificate No. 1196040, MKI V 07 V 7/083, Publ. 07.12.85, Byul. No. 45.
4. A. N. Petunin, *Methods and Techniques for Gas-Flow Measurement* [in Russian], Mashinostroenie, Moscow (1972).
5. D. C. Wilcox, "Reassessment of the scale determining equation for advanced turbulence models," *AIAA J.*, **32**, No. 11, 1299–1310 (1988).
6. A. J. Chorin, "Numerical solution of Navier–Stokes equation," *Math. Comput.*, **22**, 745–762 (1968).
7. R. Peyret and T. D. Taylor, *Computational Methods for Fluid Flow*, Springer Verlag, New York (1983).
8. S. V. Patankar, *Numerical Heat Transfer and Fluid Flow*, Hemisphere–McGraw Hill, Washington–New York (1980).
9. C. Fletcher, *Computational Techniques for Fluid Dynamics*, Springer-Verlag, Heidelberg (1988).
10. A. V. Shvab and V. N. Brendakov, "Numerical simulation of a swirled flow on the basis of a three-parameter turbulence model," *Izv. Vyssh. Uchebn. Zaved., Fizika*, No. 10, 120–123 (2004).
11. A. Singh, B. D. Vyas, and U. S. Powle, "Investigations on inward flow between two stationary parallel disks," *Int. J. Heat Fluid Flow*, No. 20, 395–401 (1999).